Frequency domain analysis of noise in simple gene circuits

Chris D. Cox[a)]
Department of Civil and Environmental Engineering, University of Tennessee, Knoxville, Tennessee 37996 and Center for Environmental Biotechnology, University of Tennessee, Knoxville, Tennessee 37996

James M. McCollum
Department of Electrical and Computer Engineering, University of Tennessee, Knoxville, Tennessee 37996

Derek W. Austin
Siemens Molecular Imaging, Knoxville, Tennessee 37932

Michael S. Allen
Molecular-Scale Engineering and Nanoscale Technologies Research Group, Oak Ridge National Laboratory, Oak Ridge, Tennessee 37831-6006; Center for Environmental Biotechnology, University of Tennessee, Knoxville, Tennessee 37996; and Department of Materials Science, University of Tennessee, Knoxville, Tennessee 37996

Roy D. Dar
Molecular-Scale Engineering and Nanoscale Technologies Research Group, Oak Ridge National Laboratory, Oak Ridge, Tennessee 37831-6006 and Department of Physics, University of Tennessee, Knoxville, Tennessee 37996

Michael L. Simpson[b)]
Molecular-Scale Engineering and Nanoscale Technologies Research Group, Oak Ridge National Laboratory, Oak Ridge, Tennessee 37831-6006; Department of Materials Science, University of Tennessee, Knoxville, Tennessee 37996; and Center for Environmental Biotechnology, University of Tennessee, Knoxville, Tennessee 37996

(Received 30 January 2006; accepted 21 April 2006; published online 30 June 2006)

Recent advances in single cell methods have spurred progress in quantifying and analyzing stochastic fluctuations, or noise, in genetic networks. Many of these studies have focused on identifying the sources of noise and quantifying its magnitude, and at the same time, paying less attention to the frequency content of the noise. We have developed a frequency domain approach to extract the information contained in the frequency content of the noise. In this article we review our work in this area and extend it to explicitly consider sources of extrinsic and intrinsic noise. First we review applications of the frequency domain approach to several simple circuits, including a constitutively expressed gene, a gene regulated by transitions in its operator state, and a negatively autoregulated gene. We then review our recent experimental study, in which time-lapse microscopy was used to measure noise in the expression of green fluorescent protein in individual cells. The results demonstrate how changes in rate constants within the gene circuit are reflected in the spectral content of the noise in a manner consistent with the predictions derived through frequency domain analysis. The experimental results confirm our earlier theoretical prediction that negative autoregulation not only reduces the magnitude of the noise but shifts its content out to higher frequency. Finally, we develop a frequency domain model of gene expression that explicitly accounts for extrinsic noise at the transcriptional and translational levels. We apply the model to interpret a shift in the autocorrelation function of green fluorescent protein induced by perturbations of the translational process as a shift in the frequency spectrum of extrinsic noise and a decrease in its weighting relative to intrinsic noise. © *2006 American Institute of Physics*.
[DOI: 10.1063/1.2204354]

Stochastic fluctuations, or "noise," in gene circuits arise due to the random timing of biochemical reactions within a cell and the discrete nature of the molecular populations affected by these reactions. The noise can originate from variations in the global resources (e.g., polymerases, ribosomes, nucleic and amino acids) utilized in transcription and translation (called "extrinsic noise") or within the transcriptional and translational processes themselves (called "intrinsic noise"). Not only have cells evolved to maintain fidelity of gene function in the presence of noise, there are many examples in which cells exploit noise-driven phenotypic diversity to achieve a desired end. Further, the manner in which noise propagates through a gene circuit allows certain inferences about the gene circuit architecture. In recent years a number of theoretical and experimental studies have been undertaken to characterize the sources and propagation of

[a)]Electronic mail: ccox9@utk.edu
[b)]Electronic mail: simpsonml1@ornl.gov

noise in gene networks. Most of these studies have focused on quantifying and interpreting the magnitude of the noise as quantified by distributions or statistics of a noise-affected output within a population of cells. We have developed a frequency domain (FD) approach that captures information about both the magnitude of stochastic fluctuations and their timing within individual cells and demonstrates that the timing plays a critical role in gene circuit performance. Here we review recent advances in characterizing noise in gene circuits, describe the analytical and experimental aspects of the FD approach, and demonstrate its application to the analysis of intrinsic and extrinsic noise in transcription and translation processes.

I. INTRODUCTION

In 1940 the physicist Max Delbruck recognized that small populations of enzyme molecules within a cell would give rise to statistical fluctuations in biochemical reactions and that these fluctuations could have profound impacts on cell physiology.[1] He later proposed that fluctuations of this type could explain the variation in the number of viruses produced upon lysis of infected bacteria.[2] In the following decades many examples of the importance of stochastic fluctuations in gene regulation have been reported. Prokaryotic examples include regulation of *lac* expression at low levels of induction,[3] the lysis-lysogeny decision in phage-λ,[4,5] and the swimming and tumbling periods of bacteria during chemotaxis.[6] Examples of stochastically driven phenotype variability in eukaryotes include variability in the response to mating pheromone in yeast[7] and the notch-mediated epidermal-neural decision in *Drosophila* neuro-ectoderm.[8] Recent studies have also suggested that stochastically driven phenotype diversity in a clonal population may ensure that a few cells remain poised to exploit changing environmental conditions,[9] thereby improving fitness.

Stochastic fluctuations (hereafter referred to as noise) are introduced into the populations of mRNA, protein, and other molecular species by several sources. The random timing and discrete nature (i.e., integer number of molecules) of molecular events such as transcription, translation, multimerization, and protein/mRNA decay processes lead to a noise component that is intrinsic to a local gene circuit or pathway.[5,10,11] Conversely, fluctuations in RNAP, ribosomes, transcription factors, or other cellular molecular machinery shared by gene circuits or pathways lead to an extrinsic noise component.[12,13] The difference between intrinsic and extrinsic noise is not just one of definitions, as these fluctuations have different sources, attributes, and consequences (Fig. 1). For example, although intrinsic noise in one gene circuit is uncorrelated with that in any other gene circuit, extrinsic noise is correlated across gene circuits as it arises from shared cellular resources. Further, this sharing of resources and transmission of fluctuations provides for a coupling between gene circuits that have no direct regulatory relationship.[14] That is, a high demand for expression by one pathway can affect the rate at which an unrelated pathway is expressed.

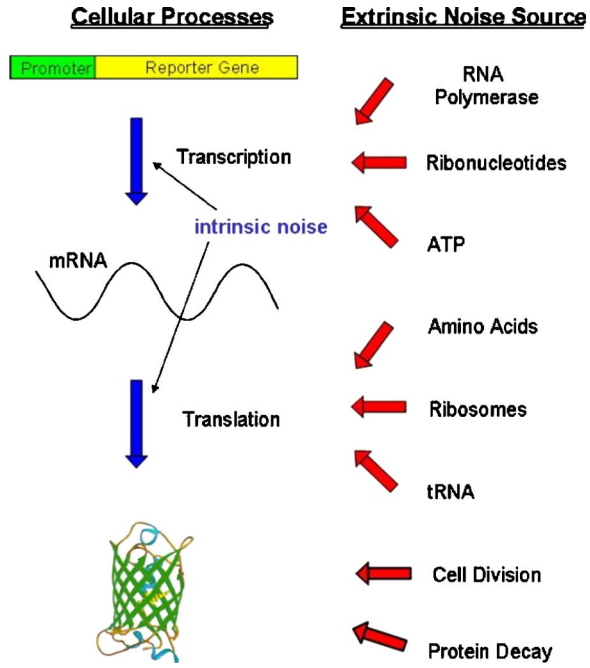

FIG. 1. (Color online) Intrinsic noise sources originate from the transcription and translation processes affecting a single gene, whereas extrinsic noise sources affect all genes within the cell.

Over the last few years there has been a great deal of focus on the theory, analysis, modeling, and simulation of stochastic fluctuations in gene circuits and networks.[5,7,10,13,15–26] The most rigorous and accurate mathematical representation for calculating the discrete stochastic time evolution of a reacting system is the chemical master equation (CME), which describes how the overall probability of any state in the system evolves over time as a result of various possible chemical reactions.[18] Unfortunately, the CME approach becomes impractical for genetic circuits and networks of even moderate complexity. A tractable method of dealing with discrete stochastic simulations is exact stochastic simulation;[16,17] however, although simulation is an invaluable aide in understanding stochastic fluctuations in genetic systems, it is difficult to extract fundamental relationships between gene circuits parameters (e.g., kinetic rates) and function using simulation alone. Instead, such relationships have most often been predicted through mathematical analysis using approaches (e.g., Fokker-Planck and Langevin) that are simplifications of the CME.[19,22,24,25,27]

Coupled with the progress in gene circuit noise theory, analysis and simulation, there has been significant experimental progress. Elowitz *et al.* used the correlation of yellow and cyan fluorescent proteins under the control of identical promoters at different locations within the genome for the independent measurement of the extrinsic and intrinsic noise components described earlier, and showed that the contribution of extrinsic noise to total noise may be larger than that of intrinsic noise.[12] Blake *et al.* measured gene circuit noise in eukaryotes and showed the effect of transcription reinitiation on the magnitude of the stochastic fluctuations.[28] Raser and O'Shea extended the study of extrinsic and intrinsic noise to eukaryotic gene expression by quantifying differ-

ences of expression from two alleles in diploid yeast cells.[29] They demonstrated that extrinsic noise was also dominant in two wild-type yeast genes and that slow rates of promoter state transition could dominate intrinsic noise as predicted by theoretical studies.[21,25] Similarly, Becskei *et al.* further demonstrated that noise associated with low molecular number transcripts in yeast was not the result of the low populations per se, but rather resulted from relatively rare gene activation events.[30] Rosenfeld *et al.* used time-lapse microscopy to track reporter gene activity response to an inducer over multiple cell generations.[31] They resolved the autocorrelation function of the gene response into contributions from rapidly decaying intrinsic noise and more persistent extrinsic noise that decays over approximately one cell cycle. Pedraza and van Oudenaarden used cross correlation of three fluorescent reporter genes to determine how intrinsic and extrinsic noise propagates through gene cascades.[14] The synthetic cascade was tunable via the concentrations of two inducers. A calibrated analytical model of the cascade correctly predicted changes in noise response as a function of changing inducer concentrations. However, all of these experimental studies focused on noise magnitudes, and like their theoretical counterparts, largely ignored the frequency content of this noise.

Most of these theoretical and experimental investigations have dealt with noise magnitude using stochastic distributions (e.g., means, variances, standard deviations) of the molecular populations at steady state, largely ignoring the rate of the fluctuations. In contrast, we have employed a FD approach to analysis and experimentation that deals with the noise spectra content. In this approach the noise sources have a flat (i.e., equal power at all frequencies or white) spectrum, but these spectra are shaped as the noise propagates from the sources to molecular populations or concentrations of interest. As a result, there is a mapping between the spectral content of gene expression fluctuations and the structure and function of the underlying gene circuits.

Our FD analysis has demonstrated that the frequency content of the noise may have important implications for gene regulation and function that are not captured by analysis or measurement of noise magnitudes.[24–26] For example, our analysis predicts that kinetic parameters are reflected in the noise frequency range and that negative autoregulation not only reduces the magnitude of the noise, but also shifts the remaining noise to higher frequencies where it may have little or no regulatory effect.

Unfortunately, it is more difficult to perform FD measurements as these require relatively long time series measurements from individual cells. Consequently flow cytometry, which has been a very productive tool for measuring stochastic distributions, cannot be used for FD measurements. However, we recently measured stochastic fluctuations in reporter gene expression of growing cells using time-lapsed microscopy.[32] We measured noise frequency content in growing cell cultures and verified our theoretical prediction[24] that in addition to noise magnitude, gene circuits manipulate noise spectra, impacting the fate and regulatory effect of the noise as it propagates through the gene network.[32] We verified our prediction[24] of the shift of noise spectra to higher frequencies and the link between gene circuit structure and the resulting noise frequency range and showed that changes in gene circuit parameters, such as cell growth and protein decay rates, modulate the noise frequency range distributions.[32] Further, these results showed that measured noise frequency range distributions combined with stochastic simulations can be used to probe mechanistic details of molecular interactions within gene circuits.[32]

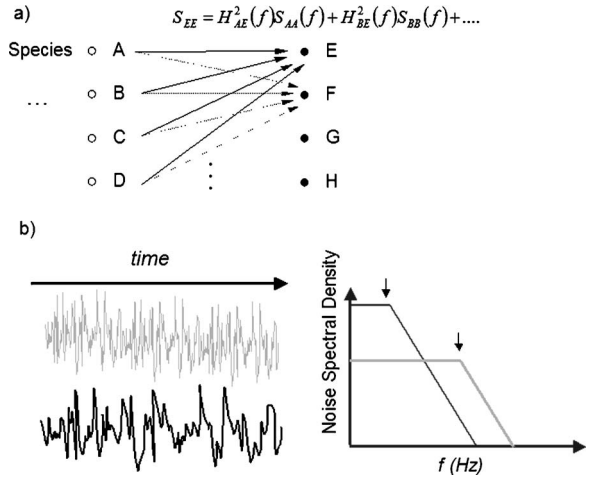

FIG. 2. Basic concepts in frequency domain analysis. (a) Chemical species A–H are represented as nodes, each of which represents a noise source with its own characteristic PSD. Noise power transfer functions describe the effect of upstream noise sources (A–D) on downstream output nodes (E–H). For example, the noise source at A is characterized by its PSD $S_{AA}(f)$ and its effect on output E is given by $H^2_{AE}(f)\ S_{AA}(f)$. (b) Stochastic time series generated by noise sources (left) are characterized by their power spectral densities (right). The grey and black curves represent high and low frequency noise sources, respectively. The vertical arrows indicate locations of pole frequencies.

Here we review FD analytical and experimental techniques and our previous results. In addition, we present a model that explicitly considers extrinsic noise sources emanating from the transcriptional and translational level and use the model for the interpretation of our experimental results where noise was significantly affected by perturbation of translational processes.

II. FREQUENCY DOMAIN ANALYSIS: TOOLS FOR GENE CIRCUIT ARCHITECTURAL ANALYSIS

Our FD approach is equivalent to the chemical Langevin analysis and is applicable to linear systems and nonlinear systems for which linear approximations are sufficiently accurate over conditions of interest. In the FD approach the genetic/biochemical system is conceptualized as a chemical circuit with nodes for each chemical species, and the noise is generated by a set of noise sources [Fig. 2(a)]. The noise sources are characterized by their power spectral densities (PSDs), which describe how the noise is distributed in frequency space [Fig. 2(b)]. The PSD of the noise in the concentration (or population) of chemical species i ($S_i(f)$) is found from the weighted sum of the noise sources according to

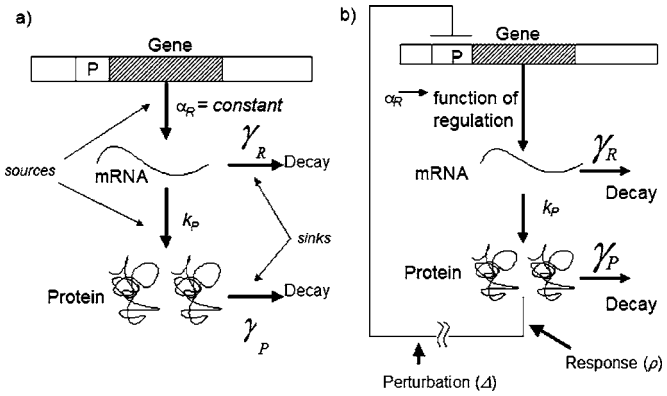

FIG. 3. Model of single gene expression. (a) noise sources include synthesis of mRNA molecules from the template DNA strand at rate α_R, and translation of proteins at a rate $k_P \cdot \mathrm{mRNA}(t)$. Noise sinks include decay of mRNA and protein with first-order rate constants γ_R and γ_P, respectively. (b) The same as (a) except that the protein is negatively autoregulated. The loop transmission T is calculated by breaking the loop at any convenient point, introducing a perturbation (Δ) just to the downstream side of the break, measuring the response (ρ) that returns to the upstream side of the break and calculating $T=\rho(f)/\Delta(f)$. Figure from Ref. 24.

$$S_i(f) = \sum_{j=1}^{G} |H_{ij}^2(f)| S_j(f) = \sum_{j=1}^{G} |H_{ij}^2(0)| S_j(0) f_{N\_ij}, \tag{1}$$

where f is the frequency (Hz), $S_j(f)$ is the PSD of noise source j, G is the number of noise sources contributing to noise in chemical species i, $|H_{ij}^2(f)|$ is the noise power transfer function between the noise source j and chemical species i, and f_{N_ij} is a characteristic frequency range (known as the noise bandwidth) of the noise in species i due to source j. The noise power transfer functions are found from

$$|H_{ij}^2(f)| = \left(\frac{\partial |x_i(f)|}{\partial |r_j(f)|} \right)^2, \tag{2}$$

where $|x_i(f)|$ is the magnitude of fluctuations at frequency f in the concentration of species i due to fluctuations in molecular populations at frequency f caused by noise source j ($r_j(f)$).

The noise sources are well described by shot noise with a wide band (compared to the frequency limitations of the gene circuit) white spectrum.[24] Shot noise is the noise that originates from the discrete nature of the signal carrier. The PSD of shot noise arising from a Poisson process is proportional to the average flux (k_T) through the process such that[24]

$$S_j(f) = 2k_T, \tag{3}$$

where $S_j(f)$ is the single-sided (positive frequency only) PSD of the noise source j. At steady state the noise sources are found in pairs [a source and a sink; Fig. 3(a)] at the points of molecular transitions (synthesis, decay, polymerization, complex formation, etc.), so the total PSD for a pair of noise sources at location j is

$$S_{j\_\mathrm{total}}(f) = 4k_T. \tag{4}$$

The noise power transfer functions in genetic circuits will be of the form

$$|H_{ij}(f)|^2 = H_{ij}^2(0) \frac{\prod_{n=1}^{n_{j,k}} \left(1 + \left(\frac{f}{f_{zn\_ij}} \right)^2 \right)}{\prod_{m=1}^{m_{j,k}} \left(1 + \left(\frac{f}{f_{pm\_ij}} \right)^2 \right)}, \tag{5}$$

where $f_{z1,\ldots,n}$ (zeros) and $f_{p1,\ldots,m}$ (poles) are frequencies associated with the kinetic parameters of the reactions between noise source j and chemical species i. The transfer function describes how noise is modified as it propagates through the circuit. Below the first pole frequency, the PSD is flat and the noise power is independent of frequency. As the frequency increases above the first pole, the noise power decreases with $1/f^2$. The noise power decreases by an additional factor of $1/f^2$ for each additional pole encountered [Fig. 2(b)]. Most reactions generate only poles, although zeros are seen in reversible reactions.[26] Zeros have the opposite effect of poles: noise power increases with f^2 at frequencies above the zero frequency. Overall, the change in noise power with frequency can be described by $f^{2(nz-np)}$ where nz and np are the number of zeros and poles with characteristic frequencies less than f. Note that the PSD of the sources are flat and featureless [Eq. (4)], but the PSDs in the species concentrations have structure created by the kinetic parameters of the reactions [Eq. (1)].

The noise power transfer functions are derived from the linearization and Fourier or Laplace transformation of the ordinary differential equations describing the system. Therefore FD analysis has most of the same limitations and caveats as the Langevin approach.[19] One notable exception is that the FD approach can be used for some cases of very low molecular populations where the time domain Langevin approach fails.[25] Further, some limitations are overstated in the literature. As has been demonstrated with electronic circuits for quite some time, FD techniques can be applied to some nonlinear systems. However, such applications must be handled with care and the results scrutinized.

III. APPLICATION OF FD ANALYSIS

A. Single gene circuit

Figure 3(a) is a schematic diagram of an unregulated single gene system. Considering only the intrinsic noise, the Langevin equations for this system are

$$\begin{aligned} \frac{dr}{dt} &= -(\gamma_R + \delta) r + \alpha_R(t) + \eta_R, \\ \frac{dp}{dt} &= -(\gamma_P + \delta) p + k_P r + \eta_P, \end{aligned} \tag{6}$$

where r and p are mRNA and protein concentrations, γ_R and γ_P are mRNA and protein decay rate constants, δ is the rate of dilution due to growth, α_R is the transcription rate, k_P is the translation rate constant, and η_R and η_p are random variables that represent the noise. At steady state the average mRNA ($\langle r \rangle$) and protein ($\langle p \rangle$) concentrations found from Eqs. (1) and (2) are $\alpha_R/(\gamma_R+\delta)$ and $\alpha_R k_P/((\gamma_R+\delta)(\gamma_P+\delta))$, respectively. As the typical half-life of mRNA (2–5 min)[33] is

much less than the cell doubling time, we will make the approximation $\gamma_R + \delta \approx \gamma_R$.

From Eq. (4) the PSDs of the mRNA (S_{RR}) and protein (S_{PP}) synthesis and decay noise are

$$S_{RR} = 4\alpha_R, \qquad S_{PP} = 4\frac{\alpha_R k_P}{\gamma_R}. \tag{7}$$

The signal and noise power transfer functions from the point of mRNA ($H_R(f)$) and protein ($H_P(f)$) synthesis to the reporter protein output are found by Fourier transform and solution of the Langevin equations to obtain[24]:

$$H_R(f) = \frac{b}{\gamma_P + \delta}\frac{1}{\left(1 + i\frac{f}{f_{\text{mRNA}}}\right)\left(1 + i\frac{f}{f_{\text{protein}}}\right)}, \qquad H_P(f) = \left(\frac{1}{\gamma_P + \delta}\right)^2 \frac{1}{\left(1 + \left(\frac{f}{f_{\text{protein}}}\right)^2\right)}, \tag{8}$$

$$|H_R(f)|^2 = \frac{\left(\frac{b}{\gamma_P + \delta}\right)^2}{\left(1 + \left(\frac{f}{f_{\text{mRNA}}}\right)^2\right)\left(1 + \left(\frac{f}{f_{\text{protein}}}\right)^2\right)}, \qquad |H_P(f)|^2 = \frac{\left(\frac{1}{\gamma_P + \delta}\right)^2}{\left(1 + \left(\frac{f}{f_{\text{protein}}}\right)^2\right)}, \tag{9}$$

where the pole frequencies are associated with mRNA ($f_{\text{mRNA}} = \gamma_R/2\pi$) and protein ($f_{\text{protein}} = (\gamma_p + \delta)/2\pi$) decay, and the term b ($=k_P/\gamma_R$; often referred to as the burst rate) is the average number of proteins produced from each mRNA transcript. The power transfer functions [Eq. (9)] can be understood in terms of the gain (numerator) and the frequency modification (denominator) as the noise propagates through the circuit. The gain for transcriptional noise sources is greater by a factor of b^2. Simple transcription-translation circuits behave as low-pass filters, as noise becomes negligible at frequencies greater than the pole frequencies. As the effect of a noise source decreases at $1/f^2$ for frequencies higher than the first pole, other poles are often neglected in multipole systems. As mRNA typically decays much faster than the protein ($\gamma_R \gg \gamma_P$), the mRNA pole may be neglected with little error and the single pole noise bandwidth approximation can be used.[24] With this simplification, the noise bandwidth (range of frequencies that have a significant noise content; Δf_N) for both noise sources can be approximated as[24]

$$\Delta f_N \approx \frac{\pi}{2} f_{\text{protein}} = \frac{\gamma_p + \delta}{4}, \tag{10}$$

and the variance of the output (protein population) noise is given by

$$\sigma_P^2 \approx (H_R^2(0)S_{RR} + H_P^2(0)S_{PP})\Delta f_N = \langle p \rangle (1 + b), \tag{11}$$

where we have used the relationships for $\langle p \rangle$ and b defined earlier.

The noise figures of merit are

$$\frac{\sigma_P^2}{\langle p \rangle} = 1 + b, \tag{12}$$

$$\frac{\sigma_P}{\langle p \rangle} = \sqrt{\frac{(1+b)}{\langle p \rangle}}. \tag{13}$$

Equation (12) gives the noise strength and Eq. (13) gives the coefficient of variation (CV) with results that are in agreement with previous analysis.[22,23] However, the FD approach shows that this noise is spread over a frequency range related to Δf_N and controlled by the protein decay and dilution rate.

The previous analysis provides a relationship that can be used to aide the analysis of multigene systems. For a constitutively expressed gene circuit

$$S_p^i(f) \approx \frac{4b\langle p \rangle}{\delta + \gamma_p}\left(\frac{1}{1 + \left(\frac{2\pi f}{\delta + \gamma_p}\right)^2}\right), \tag{14}$$

where $S_p^i(f)$ is the intrinsic noise in the protein concentration, we have neglected the mRNA pole, and we have assumed that $b + 1 \approx b$.

B. Transcriptional control

In many prior analyses transcriptional control was approximated using a Hill expression:[23,24,34,35]

$$I = \frac{1}{1 + (d/K_h)^n}, \tag{15}$$

where I is the induction level of the gene, d is the concentration of a regulatory molecule, K_h is a constant that indicates the value of d at which the induction level reaches 0.5, and n is the Hill coefficient. Positive and negative values of n correspond to repression and induction, respectively. Although this approach may reasonably approximate the static deterministic behavior of transcriptional regulation, it can lead to significant errors by neglecting both the dynamics (frequency response) and the noise of transcriptional regulation. A more realistic description would include switching between discrete high and low transcriptional rates with the average rate determined by the fractional amount of time spent in each of the two states. This model is consistent with transcription controlled through protein-DNA interactions at an operator site within the gene promoter region. We performed a FD analysis of the case of a single operator site within a single copy of the operon as shown in Fig. 4. In this analysis we considered two possible states, denoted as O (unbound) and O' (bound), and transition between these states was described by

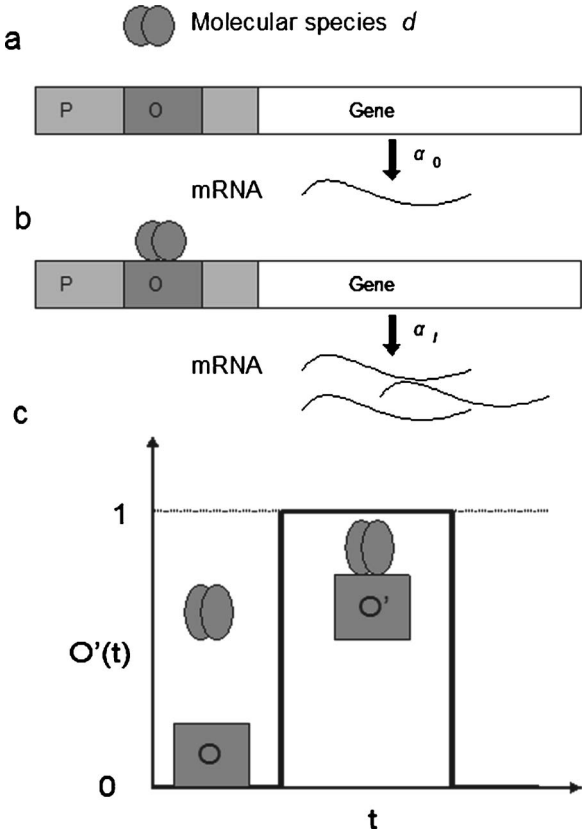

FIG. 4. Model of gene regulation. (a) Gene in basal state (O) with operator unbound by molecular species d and producing transcripts at slow rate. (b) Gene in induced state (O') with molecular species d bound to operator and producing transcripts at increased rate. (c) The operator transitions between state O and O' as a function of time. The level of induction is given by the fractional time the gene spends in state O'. Operator dynamics are characterized by the average time the operator remains in each state prior to transitioning. Figure from Ref. 25.

$$O \xrightarrow{k_f d} O', \qquad O' \xrightarrow{k_r} O, \tag{16}$$

where k_f and k_r are rate constants for the forward and reverse reactions, respectively, and d is the population of the molecular species that controls transcription by binding with O. Equation (16) applies to both positive and negative regulation as the fully induced state may be either O or O'. As our previous analysis treated positive regulation,[25] here we consider only the negatively regulated case ($O' \rightarrow$ minimally induced). These results can be directly applied in the analysis of negative autoregulation that follows.

As there is only one operator site, the population of the unbound operator, $O(t)$, is either one or zero at all times. For negative regulation we define

$$\alpha(t) = \alpha_I, \quad O = 1, \tag{17a}$$

$$\alpha(t) = \alpha_0, \quad O = 0, \tag{17b}$$

$$\alpha_R = \alpha_0[1 - O(t)] + \alpha_I \overline{O(t)} = \alpha_0 + (\alpha_I - \alpha_0)\overline{O(t)}, \tag{17c}$$

where $\alpha(t)$, α_0, α_I, and α_R are the instantaneous, basal, fully induced, and average transcription rates respectively, and $\overline{O(t)}$ is the time-averaged value of $O(t)$.

As individual transcription events and $O(t)$ are uncorrelated random processes, the autocorrelation function for the gated term in Eq. (17c), $\Phi_{O\alpha}(\tau)$, is given by

$$\Phi_{O\alpha}(\tau) = \Phi_O(\tau)\Phi_\alpha(\tau), \tag{18}$$

where $\Phi_O(\tau)$ is the autocorrelation function for $O(t)$ and $\Phi_\alpha(\tau)$ is the autocorrelation function for a random series of impulse functions (average rate$=\alpha_I-\alpha_0$) corresponding to mRNA synthesis.[25] The PSD of the noise in the mRNA synthesis rate is found by summation of the PSDs of mRNA decay noise (equal in magnitude, but uncorrelated to synthesis shot noise[24]), the wideband white noise of the constant term (i.e., basal gene expression) in Eq. (17c), and the gated noise of Eq. (18) to yield:[25]

$$\begin{aligned} S_{RR\_\mathrm{reg}}(f) &= 4(\alpha_0 + \overline{O(t)}(\alpha_I - \alpha_0)) \\ &\quad + \frac{4(\alpha_I - \alpha_0)^2(\overline{O(t)} - (\overline{O(t)})^2)}{(k_r + k_f d)} \\ &\quad \times \left(\frac{1}{1 + \left(\frac{2\pi f}{(k_r + k_f d)} \right)^2} \right) \\ &= 4\alpha_R + \frac{4\alpha_R^2 \left(\frac{1}{\overline{O(t)}} - 1 \right)}{(k_r + k_f d)} \left(\frac{1}{1 + \left(\frac{2\pi f}{(k_r + k_f d)} \right)^2} \right), \end{aligned} \tag{19}$$

where the subscript _reg denotes the regulated case and the PSD of the gated noise term was found by direct calculation and then Fourier transformation of the autocorrelation function of Eq. (18).[25] The first term in Eq. (19) is the PSD of the noise source associated with the average transcription rate, whereas the second term accounts for variations around the average transcription rate caused by the operator. The operator component increases at low induction levels [low values of $\overline{O(t)}$] and for slow operator dynamics [low values of $(k_r + k_f d)$]. Noise from slow operator dynamics is limited to low frequencies by the presence of the filtering action of the pole in Eq. (19).

The dynamics of this transcriptional regulation were also analyzed to show that the transfer function, $H_o(f)$, from concentration of species d to the transcription rate is given by[25]:

$$H_{O'}(f) = -\frac{(k_r k_f)/(k_r + k_f\langle d\rangle + k_f)}{(k_r + k_f\langle d\rangle)} \left(\frac{1}{1 + i\dfrac{2\pi f}{(k_r + k_f\langle d\rangle + k_f)}} \right), \tag{20}$$

where $\langle d\rangle$ is the average concentration of species d.

This analysis shows that there are at least two major shortcomings when using a Hill function to approximate transcription regulation for stochastic analysis. The first term on the right-hand side (rhs) of Eq. (19) is a shot noise term[24] and the only noise present when the Hill expression is used.

The second term on the rhs of Eq. (19) is an additional noise term (operator noise) found from this more realistic treatment of transcriptional regulation[21,25] and may be the dominant source of transcriptional noise. Further, the Hill expression assumes that changes in the transcription factor concentration are immediately reflected in the transcription rate, whereas Eq. (19) shows that this response is limited by the operator dynamics.

C. Autoregulated gene circuit

Autoregulation, or feedback, exists when the level of an output of a gene circuit regulates the rate at which this output is generated. To deal with autoregulation we applied the electronic feedback concept of loop transmission to gene circuit analysis. The loop transmission, T, is the transfer function around the loop, or the frequency dependent first derivative of the regulation strength. It may be thought of as a measure of the resistance of the circuit (electronic or biochemical) to variation from the steady state. T is calculated by breaking the loop at any convenient point [e.g., at the point of transcriptional regulation; Fig. 3(b)], introducing a perturbation (Δ) just to the downstream side of the break [e.g., a small change in transcription rate; Fig. 3(b)] and measuring the response (ρ) that returns to the upstream side of the break [e.g., the change the circuit would make in transcription rate; Fig. 3(b)]. $T(f)$ is given by $\rho(f)/\Delta(f)$, and the sign of $T(0)$ is negative (resists fluctuations) for negative autoregulation and is positive (reinforces fluctuations) for positive autoregulation. For the gene circuit of Fig. 3(b):

$$\begin{aligned} T(f) &= H_R(f)H_o(f) \\ &= \frac{-H_R(0)H_o(f)}{\left(1+i\frac{f}{f_{\text{protein}}}\right)\left(1+i\frac{f}{f_{\text{mRNA}}}\right)} \\ &= \frac{T(0)}{\left(1+i\frac{2\pi f}{\gamma_P}\right)\left(1+i\frac{2\pi f}{\gamma_R}\right)\left(1+i\frac{2\pi f}{(k_r+k_f d_0+k_f)}\right)}, \end{aligned} \tag{21}$$

where $T(0)=-H_R(0)H_o(0)$, and the other terms are as described previously.

Here we consider transcriptional regulation where the protein product of the gene circuit negatively regulates the transcription rate by binding to an operator site in the promoter. We make the simplifying assumption that the operator dynamics are fast compared to the protein decay and dilution rates and approximate mRNA synthesis noise by modifying Eq. (19) such that

$$S_{RR\_\text{reg}}(f) = 4\alpha_R + \frac{4\alpha_R^2\left(\frac{1}{\overline{\overline{O(t)}}}-1\right)}{(k_r+k_f d)}. \tag{22}$$

The protein synthesis noise found by modifying Eq. (7) to account for the negative regulation mediated decrease of the protein synthesis rate to obtain

$$S_{pp\_\text{reg}}(f) = 4k_p\langle\text{mRNA}\rangle = \frac{4k_p\alpha_R}{\gamma_R} = 4b\alpha_R. \tag{23}$$

The noise in the protein concentration may be found by the application of Eq. (9), but the transfer functions and the noise bandwidth have been altered by the negative autoregulation such that[24]

$$\begin{aligned} |H_{R\_\text{reg}}(0)|^2 &= \frac{1}{(H_o(0))^2}\left(\frac{-T(0)}{1-T(0)}\right)^2 \\ &= \frac{1}{(H_o(0))^2}\left(\frac{H_R(0)H_o(0)}{1-T(0)}\right)^2 \\ &= \frac{H_R^2(0)}{(1-T(0))^2}, \\ |H_{P\_\text{reg}}(f)|^2 &= \left(\frac{1}{bH_o(0)}\right)^2\left(\frac{-T(0)}{1-T(0)}\right)^2 \\ &= \frac{1}{(bH_o(0))^2}\left(\frac{H_R(0)H_o(0)}{1-T(0)}\right)^2 \\ &= \frac{1}{b^2}\left(\frac{H_R(0)}{1-T(0)}\right)^2, \end{aligned} \tag{24}$$

and

$$\Delta f_N \approx (1-T(0))f_{\text{protein}} = (1-T(0))\frac{\gamma_p}{4}, \tag{25}$$

where _reg denotes a transfer function for the negatively autoregulated case and the other parameters are as previously described. Comparison of Eqs. (25) and (10) reveals that negative autoregulation extends the noise bandwidth by a factor of $(1-T(0))$, as $T(0)$ is negative. The increase in bandwidth occurs by shifting some of the noise to higher frequencies where it may subsequently be filtered out by downstream circuit elements.[24] Then,

$$\begin{aligned} \sigma_P^2 &\approx (|H_{R\_\text{reg}}(0)|^2 S_{RR\_\text{reg}} + |H_P(0)|^2 S_{PP\_\text{reg}})\Delta f_N \\ &= \frac{\langle p\rangle}{(1-T(0))}\left((b+1)+\frac{b\alpha_R\left(\frac{1}{\overline{\overline{O(t)}}}-1\right)}{(k_r+k_f\langle p\rangle)}\right) \end{aligned} \tag{26}$$

and

$$\left(\frac{\sigma_{P\_\text{reg}}^2}{\langle p_{\text{reg}}\rangle}\right) = \frac{\left(\frac{\sigma_P^2}{\langle p\rangle}\right)}{(1-T(0))} + \frac{b\alpha_R\left(\frac{1}{\overline{\overline{O(t)}}}-1\right)}{(k_r+k_f\langle p\rangle)(1-T(0))}. \tag{27}$$

The first term in Eq. (27) shows that negative feedback decreases the noise strength of the transcriptional and translational intrinsic noise by a factor of $1/(1-T(0))$ compared to the unregulated case [Eq. (12)], which is consistent with the earlier analysis of Thattai and van Oudenaarden.[23] The second term reflects noise of operator dynamics; it is also reduced by a factor of $1/(1-T(0))$ compared to the situation where the repressor molecule population is independent of the regulated gene.

IV. EXTRINSIC NOISE

To this point we have considered only the intrinsic component of the noise. However, fluctuations in RNAP, ribosomes, transcription factors, or other cellular molecular machinery shared by gene circuits or pathways lead to an extrinsic noise component.[12,13] Measurements have shown the extrinsic noise to be large for prokaryotes[12,14,31,32] and the dominant noise component in eukaryotes.[29,36]

We recently reported a model where we approximated extrinsic noise as a single source located at the point of translation with a PSD given by[32]

$$S_E(f) \approx \frac{S_E(0)}{\left(1+\left(\frac{2\pi f}{\delta}\right)^2\right)}, \tag{28}$$

where we assumed that extrinsic noise is dominantly band limited by dilution.[31] The value of the constant term ($S_E(0)$) is set by other rates (transcription, translation, etc., of RNAP, ribosomes, proteases). For further analysis and simulation it was convenient to also collect all the intrinsic noise terms at the point of translation, resulting in a single noise source with a PSD given by

$$S_{\text{source}}(f) \approx \frac{S_E(0)}{\left(1+\left(\frac{2\pi f}{\delta}\right)^2\right)} + S_I. \tag{29}$$

These noise terms are processed by the gene circuit such that

$$S^T_{p_{m\_}N}(f) = \frac{S^E_{p_{m\_}N}(0)}{\left(1+\left(\frac{2\pi f}{\delta}\right)^2\right)\left(1+\left(\frac{2\pi f}{\delta+\gamma_p}\right)^2\right)} + \frac{S^I_{p_{m\_}N}(0)}{\left(1+\left(\frac{2\pi f}{\delta+\gamma_p}\right)^2\right)},$$
$$S^E_{p_{m\_}N}(0) + S^I_{p_{m\_}N}(0) = 1, \tag{30}$$

where $S^T_{p_{m\_}N}(f)$=the normalized ($S^T_{p_{m\_}N}(0)=1$) PSD of total noise (extrinsic+intrinsic) in the protein concentration, $S^E_{p_{m\_}N}(0)$=the normalized PSD of extrinsic noise in the protein concentration at $f=0$, and $S^I_{p_{m\_}N}(0)$=PSD of intrinsic noise in the protein concentration at $f=0$. The normalized autocorrelation function, $\Phi(\tau)$, is given by the inverse Fourier transformation of the $S^T_{p_{m\_}N}(f)$ to obtain

$$\Phi(\tau) = W_E\left(\frac{\delta+\gamma_p}{\gamma_p}e^{-\delta\tau} - \frac{\delta}{\gamma_p}e^{-(\delta+\gamma_p)\tau}\right) + W_I e^{-(\delta+\gamma_p)\tau}, \tag{31}$$

TABLE I. Reactions for simple stochastic simulation model of intrinsic and extrinsic noise in constitutive GFP circuit.

Reaction	Rate
1. $R \rightarrow R+\text{ribo}$	k_1
2. $\text{ribo} \rightarrow \text{ribo}+\text{GFP}$	$b_{\text{noise}}*\delta$
3. $\text{ribo} \rightarrow {}^*$	δ
4. $\text{GFP} \rightarrow {}^*$	$\delta+\gamma$
5. $\text{ribo}+\text{ATc} \rightarrow \text{ribo-ATc}$	k_f
6. $\text{ribo-ATc} \rightarrow \text{ribo}+\text{ATc}$	k_r
7. $\text{ribo-ATc} \rightarrow {}^*$	δ

$$W_E = \frac{\frac{S^E_{p_{m\_}N}(0)/S^I_{p_{m\_}N}(0)}{1+\left(\frac{\delta+\gamma_p}{\delta}\right)}}{\left(1+\frac{S^E_{p_{m\_}N}(0)/S^I_{p_{m\_}N}(0)}{1+\left(\frac{\delta+\gamma_p}{\delta}\right)}\right)}, \quad W_I = 1 - W_E.$$

In accordance with this analytical approach we constructed a stochastic simulation model[32] for use with simulators based on variations of the Gillespie stochastic simulation algorithm.[15,17,37,38] All extrinsic noise was collected in the ribosome concentration and was limited in frequency range by dilution. All intrinsic noise (transcription and translation) was represented by a single source at the point of translation. The reactions in the stochastic model of protein expression for a single gene circuit are given in reactions 1–4 in Table I.

Reactions 1 and 3 represent extrinsic noise that is filtered by the dilution rate. Reaction 2 represents the translation of mRNA whose stochastic variation is an intrinsic noise component that was modeled in the translation noise component. The mRNA decay rate was neglected as it is usually short compared to the dilution rate. Reaction 4 represents dilution and decay of protein. The weighting of extrinsic and intrinsic noise was set by b_{noise} according to

$$\frac{S_E(0)}{S_I} = b_{\text{noise}}, \tag{32}$$

where a value of $S_E(0)/S_I \approx 4$ is consistent with previous reports.[12,31] Note that the b_{noise} term used here does not represent the true burst rate of the system, but rather is a modeling device used only to achieve the correct ratio between extrinsic and intrinsic noise.

V. EXPERIMENTAL MEASUREMENT OF NOISE SPECTRA IN GENETIC CIRCUITS

Although there is useful information embedded within the spectral features of inherent gene circuit noise, spectral measurements are more difficult to make than noise magnitude measurements. For example, in flow cytometry sequential measurements are made on different cells and the time course of stochastic fluctuations in individual cells cannot be reconstructed. As a result, although used to great advantage in noise magnitude measurements,[22,29,34] flow cytometry is not applicable to spectral measurements.

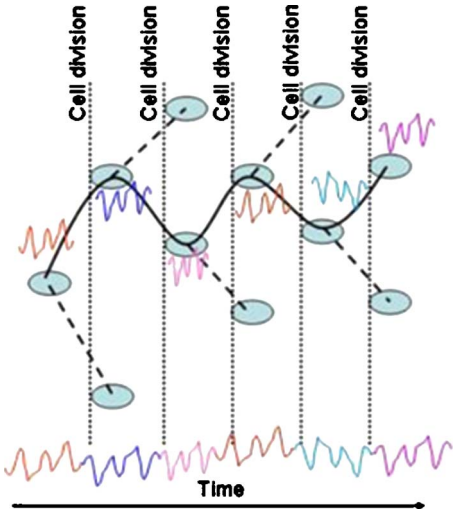

FIG. 5. (Color online) Construction of noise trajectories by sequentially combining the noise traces of cells within a common line of descent. The solid curve shows a single trajectory through five generations of cell growth and the dashed lines show alternate routes that produce other trajectories. A representative noise trace is shown next to each cell in the trajectory. The noise trace of the complete trajectory (shown at the bottom) is constructed by sequentially combining the noise traces of each cell in the trajectory. Figure from Ref. 32, supplemental material.

However, we recently[32] used time-lapse fluorescent microscopy[12] to reconstruct continuous time histories of stochastic fluctuations in growing cell cultures, thereby allowing the extraction of noise spectra. In these measurements the confocal microscope settings were adjusted to collect light (wavelength=500–550 nm) in slices (thickness $\geqslant$ cell height). Images were acquired every 5 minutes (T_s=5 min), and time series of noise in green fluorescent protein (GFP) concentrations ($X_m(n\cdot T_s)$) for individual cells $(1,2,\ldots,M)$ were defined by their differences from the population mean, and individual noise traces (trajectories) that spanned the entire growth time were constructed by sequentially combining the noise traces of cells within a common line of descent as shown in Fig. 5. Concentrations of GFP within a given experiment were assumed to be proportional to fluorescence intensity per unit cell area. Noise traces were extracted from the images for nearly all possible trajectories in each experiment, and custom MATLAB (MathWorks, Inc., Natick, MA) programs were used to find mean fluorescence of the entire cell population and to estimate population doubling time from an exponential growth curve.

Normalized autocorrelations functions (ACFs) for individual trajectories (Φ_m) were found from the noise time series ($X_m(n\cdot T_s)$) using a biased algorithm[39]

$$\Phi_m(jT_s)=\frac{\sum_{n=1}^{N-j}X_m(nT_s)X_m((n+j)T_s)}{\sum_{n=1}^{N}X_m^2(nT_s)}, \tag{33}$$

where T_s was the 5 min sampling interval, n was the sample number $(1,2,\ldots,N)$, and j had integer values from 0 to $N-1$. As the gene circuits we studied were on high copy number plasmids, it was not necessary to correct for cell-cycle variations due to chromosome replication (i.e., we assumed that plasmid concentration remained constant). The composite autocorrelation function (Φ_c) for M cell trajectories was found using

$$\Phi_c(jT_s)=\frac{\sum_{m=1}^{M}\sum_{n=1}^{N-j}X_m(nT_s)X_m((n+j)T_s)}{\sum_{m=1}^{M}\sum_{n=1}^{N}X_m^2(nT_s)}. \tag{34}$$

We investigated single gene circuits (pGFPasv) in *E. coli* TOP10 where destabilized (half-life$\approx$110 min) GFP was constitutively expressed [Fig. 6(a)]. The average GFP fluorescence, which corresponded to the concentration of mature GFP protein, was measured in individual cells in growing cultures for 4–8 h periods. The noise frequency range was defined[32] as the inverse of the time corresponding to Φ_m =0.5. Histograms of noise frequency ranges extracted from the individual trajectory autocorrelation functions [Figs. 7(a) and 7(b)] were compiled and compared with noise frequency range distributions found from exact stochastic simulation[17,38] using the extrinsic noise model described in reactions 1–4 in Table I.[32] The simulations produced as much data as 500 separate experiments, and the resulting distributions estimated the probability of finding a given noise frequency range from a randomly selected trajectory. Although some measured distributions suggested a bimodal distribution (Fig. 7), this was likely due to nonrepresentative sampling of the rare high frequency events.[32]

The analysis presented earlier predicted that protein dilution and decay rates are dominant factors defining the noise frequency range in constitutively expressed gene circuits.[24] To determine noise frequency range sensitivity to protein dilution, we varied cell growth rate for the pGFPasv circuits by controlling temperature, and in a separate experiment we changed the protein decay rate using a plasmid (pGFPaav) containing a reduced half-life ($\approx$60 min) GFP variant.[40] These perturbations to gene circuit parameters were clearly visible in the noise spectral measurements as noise frequency ranges extended to higher frequencies as a result of faster growth [Fig. 7(a)] or higher protein decay rate [Fig. 7(b)]. Although varying temperature changes the rates of all reactions, the noise frequency range of constitutively expressed circuits is largely sensitive only to protein dilution and decay rates in contrast to noise magnitude.[32]

To test our prediction of increased noise frequency range with negative autoregulation,[24] we constructed circuits with the gene for the protein TetR inserted upstream of GFP, creating a transcriptional fusion [pTetR-GFPasv; Fig. 6(b)]. This circuit was negatively autoregulated as its expression was repressed by TetR binding to operator sites in the promoter.[41] A control circuit without autoregulation was also tested, in which a chromosomal copy of tetR was constitutively expressed from the P_{N25} promoter. In both cases, repression was relieved by addition of anhydrotetracycline (ATc) to the growth medium and allowed the modulation of GFP expression.

To determine if ATc had an effect on noise spectra independent of the autoregulation of the TetR circuit, we measured the noise frequency range of the pGFPasv circuits in media supplemented with 100 ng/ml of ATc. There was a marked modification in the noise frequency range distribution [Fig. 6(c)] indicating a change in either the processing of

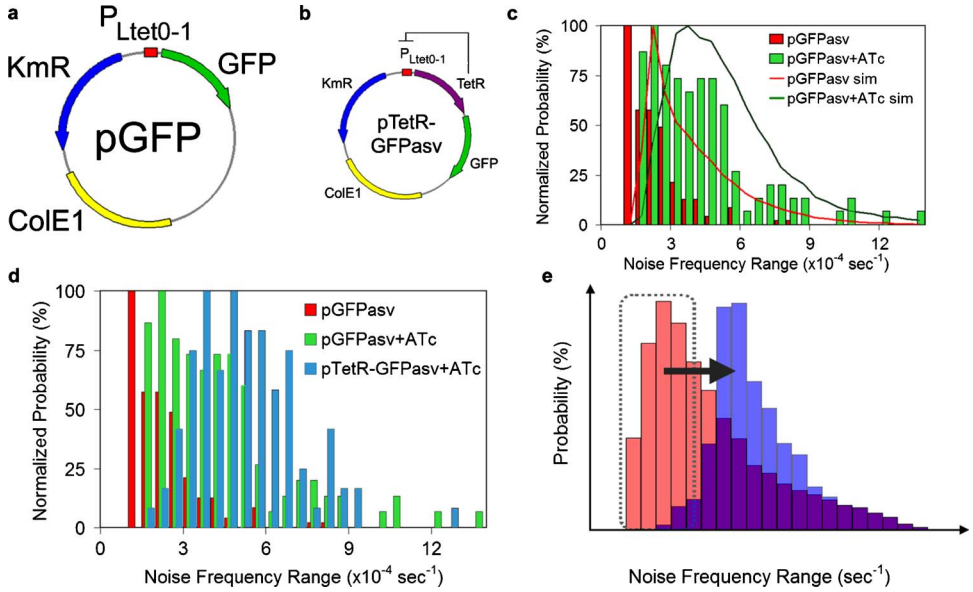

FIG. 6. (Color online) Gene circuits schematics and the effect of negative autoregulation. (a) Plasmid pGFPasv containing the constitutively expressed GFP (110 min half-life) gene circuit. (b) pTetR-GFPasv negatively autoregulated gene circuit. (c) Effect of ATc on the noise frequency range of the unregulated pGFPasv circuit (doubling time 60 min; 154 trajectories without ATc; 114 trajectories with ATc). sim., simulated using model described in Table I. (d) Negative autoregulation-mediated shift of noise frequency range (doubling time 60 min; pGFPasv: 154 trajectories without ATc, 114 trajectories with ATc; pTetR-GFPasv: 114 trajectories). (e) Model of the shift of frequency range distribution shape due to negative feedback. The right-skewed distribution shown on the left represents an unregulated circuit distribution. Negative autoregulation shifts the distribution toward the center as shown by the dashed box and arrow. The bars in dark show portions of the distribution that are common to both the regulated and unregulated circuits. The higher frequency trajectories are unaffected. Figure from Ref. 32.

the noise or the nature of the noise sources. Our modeling points to the latter with ATc inhibition of translation[42] leading to a reduction in the weighting and whitening of extrinsic noise, which we explored using the extrinsic noise simulation model in Table I. Reactions 5–7 describe the ribosome-ATc heterodimer formation and its dilution due to cell growth.[32] The frequency range distribution extracted from these simulations was compared to the measured distribution [Fig. 6(c)], with both showing a characteristic peak shift and peak broadening. Although not conclusive, this gross agreement between measured and simulated distributions supports the hypothesis that the mechanism of ATc-mediated noise frequency range modulation is an increase in high frequency content of the global extrinsic noise associated with translation and a reduction of the weighting of extrinsic noise.[32]

We measured noise frequency range distributions of pTetR-GFPasv and the control cells grown in media with 100 ng/ml of ATc. Composite noise frequency ranges of the negatively autoregulated pTetR-GFPasv exceeded those of the constitutively expressed pGFPasv in 100 ng/ml of ATc by as much as ~2–3× [Figs. 6(d) and 8], whereas the control circuits showed no noise frequency range increase (Fig. 8). The negative autoregulation-mediated noise remodeling was seen as an increase of the noise frequency range (Fig. 8) and as a modification of the shape of the distribution [Fig. 6(d)]. Autoregulation frequency response is limited by protein decay and dilution, and therefore has a larger effect on slower fluctuations than faster fluctuations. Noise trajectories that would have clustered at the lower end of the frequency range distribution in unregulated cells are pushed to higher values by negative autoregulation, whereas those in the higher frequency tail of the distribution are only weakly affected [Fig. 6(e)]. This results in frequency range distributions with a shape closer to normal distributions [Fig. 6(d)]. The frequency shift and the change in distribution shape are indicative of the presence of negative autoregulation. We would also expect a decrease in the circuit noise strength in the autoregulated gene circuit, but the variable gain of the confocal microscope did not allow for absolute measurements of noise strength.

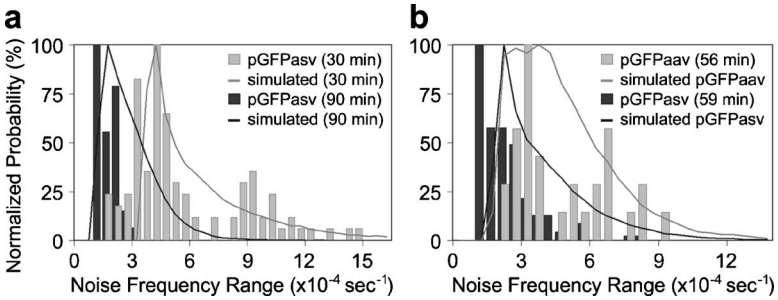

FIG. 7. Effects of cell doubling time and protein half-life on noise frequency range. Measured distributions are shown as vertical bars and simulated distributions as solid lines. (a) Shift in noise frequency range for the pGFPasv circuit as doubling time increases from ~30 min (100 trajectories; $T=32\ ^\circ C$) to ~90 min (120 trajectories; $T=22\ ^\circ C$). (b) Shift in noise frequency range as protein decay time decreases from 110 min (pGFPasv; 59-min doubling time; 154 trajectories; $T=26\ ^\circ C$) to 60 min (pGFPaav; 56-min doubling time; 33 trajectories; $T=26\ ^\circ C$). The model described in Table I was used in simulations. Figure from Ref. 32.

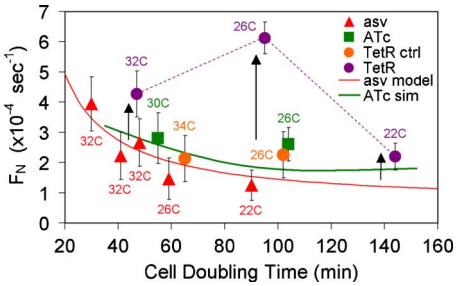

FIG. 8. (Color online) Noise frequency range vs doubling time. Measured points are shown with $\pm 1\sigma$ error bars estimated from simulation. The analytical curve [Eq. (31)] for the pGFPasv circuit and the simulated curve (Table I) for pGFPasv+100 ng ml^{-1} ATc are shown. Vertical black arrows represent regulation strength determined by the shift of the noise frequency range. The temperature (°C) of each experiment is indicated by each data point. The TetR data points are for the circuit with autoregulated tetR expression, whereas the TetR ctrl data points are for the circuit with constitutive tetR expression. Figure from Ref. 32.

These measurements validated the prediction that in addition to noise magnitude gene circuits manipulate noise spectra. We verified the link between gene circuit structure and the noise frequency range and showed that changes in gene circuit parameters (e.g., cell growth and protein decay rates) modulate the noise frequency range. Our results show a shift of noise spectra to higher frequencies and a remodeling of the noise frequency range distribution that is characteristic of negative autoregulation. This noise spectral remodeling may impact the regulatory effect of the noise as it propagates through the gene network, as higher frequency noise is more easily filtered out by downstream gene circuits in a regulatory cascade.[24] One of the more intriguing aspects of this study was that the noise frequency range distributions provided a means for evaluating a hypothesis of the mechanism of ATc-mediated remodeling of noise spectra in unregulated gene circuits. In the following section we take a closer look at the interaction of the ATc and the extrinsic noise of the gene circuit.

VI. EXTRINSIC NOISE AT THE TRANSCRIPTIONAL AND TRANSLATIONAL LEVELS

The ATc-mediated modification of the noise frequency range provides some insight into the relative contributions of extrinsic and intrinsic noise sources. Bacterial reporter protein systems studied to date are often characterized by significant extrinsic noise with an autocorrelation time scale approximately equal to the cell cycle.[31,32] For convenience, we have chosen the cell machinery components RNA polymerase (RNAP) and ribosomes to represent extrinsic noise at the transcriptional and translational levels, respectively. Other potential sources of extrinsic noise include global variation in the concentration of sigma factors, ribonucleotides, amino acids, RNases, proteases, and other shared cell resources. Although these extrinsic noise sources are not directly treated here, they are indirectly considered as there effect on the reporter gene circuit is mediated by the transcription and translation processes associated with RNAP and ribosomes. We further assume that the variation in the concentration of RNAP and ribosomes is driven by the synthesis and growth-driven dilution processes. However, their synthesis also depends upon shared cell resources which function as additional extrinsic noise sources, not considered in this model. This model also does not account for the temporary unavailability of RNAP and ribosomes actively engaged in elongation reactions to initiate new transcription and translation reactions, which causes additional variation in their free populations. We have further assumed that the series of maturation steps that nascent GFP must undergo prior fluorescence are sufficiently fast to be ignored, as discussed in Austin *et al.*[32] Despite these simplifying assumptions, the model considered here is sufficiently detailed to demonstrate the effects of transcriptional and translational-level extrinsic noise sources on the expression of GFP in the presence of ATc.

TABLE II. Reactions for model of constitutive GFP expression as affected by extrinsic noise at the transcriptional and translational level and in the presence of ATc.

RNAP polymerase synthesis and dilution (transcriptional level extrinsic noise):
$\xrightarrow{\alpha_{\mathrm{RNAP}}} \mathrm{RNAP} \xrightarrow{\delta} *$
Transcription and mRNA decay:
$\mathrm{RNAP} \xrightarrow{k_{\mathrm{tc}}} \mathrm{RNAP}+\mathrm{mRNA}$
$\mathrm{mRNA} \xrightarrow{\gamma_m} *$
Ribosome synthesis and dilution (translational level extrinsic noise):
$\xrightarrow{\alpha_{\mathrm{ribo}}} \mathrm{ribo} \xrightarrow{\delta} *$
Translation and GFP dilution/decay:
$\mathrm{mRNA}+\mathrm{ribo} \xrightarrow{k_{\mathrm{tl}}} \mathrm{mRNA}+\mathrm{ribo}+\mathrm{GFP}$
$\mathrm{GFP} \xrightarrow{\gamma_p+\delta} *$
Removal of stalled ribosomes from the cell by dilution ($k_{\mathrm{stalled}}=0$ in the absence of ATc):
$\mathrm{ribo} \xrightarrow{k_{\mathrm{stalled}}} *$

With these assumptions, we model the production of GFP according to the reactions in Table II. The last reaction is active only in the presence of ATc and its justification is described as follows. Tetracycline and many of its derivatives affect translation by binding to the 30S ribosomal subunit (reviewed in Chopra and Roberts[42]). This interaction blocks the addition of aminoacyl-tRNA and prevents translocation of the ribosome complex down the mRNA strand. In the presence of these types of translation inhibitors the mRNA is stabilized, presumably by shielding it from degradation by RNases.[43] Additionally, more recent work using untranslated RNA suggests that the increased transcription of rRNA that occurs in the presence of translation inhibitors creates a drain on RNA degradative capacity, resulting in an additional indirect protection of mRNA pools.[44]

Based on this knowledge we can summarize the action of ATc as having two effects: (1) it increases mRNA stability and (2) it causes the ribosome to stall on the transcript. Increased mRNA stability is easily handled by decreasing the mRNA decay rate γ_m. A closer look at the translation process is needed to understand the effect of a stalled ribosome. Translation is initiated upon binding of a ribosome to a ribo-

some binding site. Elongation occurs as the ribosome moves along the mRNA and produces a growing polypeptide chain, eventually producing a complete protein. The mRNA can initiate additional transcription events as soon as the ribosome clears the ribosome binding site, such that many ribosomes can be simultaneously translating a given transcript. Ribosome stalling may affect the protein production rate in two ways. First, the rate of transcript initiation may decrease as a result of a stalled ribosome blocking access to the ribosome binding site. The ribosome binding site could be blocked by a ribosome stalled directly in contact with it or stalled further down the transcript, causing a logjam. This effect can be modeled by a decrease in k_{tl} upon addition of ATc. Second, stalled ribosomes may be removed from the cell by dilution before completely translating the protein; this process is represented by the last reaction in Table II. Technically, the rate of stalled ribosome removal should be dependent on [mRNA]; however, we have ignored this dependence to simplify our frequency domain analysis as it will have only a second order effect. The effect of this reaction is to reduce the average number of proteins produced per ribosome during each cell cycle according to: $k_{\mathrm{tl}}[\mathrm{mRNA}]/(\delta + k_{\mathrm{stalled}})$.

We apply frequency domain analysis to the reactions in Table II. First, the PSD of the intrinsic noise of GFP expression $S^{i}_{\mathrm{GFP}}(f)$ can be taken directly from Eq. (14) to yield:

$$S^{i}_{\mathrm{GFP}}(f) \approx \frac{4b\langle \mathrm{GFP}\rangle}{\delta+\gamma_p}\left(\frac{1}{1+\left(\frac{2\pi f}{\delta+\gamma_p}\right)^2}\right) = \frac{4k_{\mathrm{tl}}\langle \mathrm{ribo}\rangle\langle \mathrm{GFP}\rangle}{\gamma_m(\delta+\gamma_p)}\left(\frac{1}{1+\left(\frac{2\pi f}{\delta+\gamma_p}\right)^2}\right), \tag{35}$$

where $\langle \mathrm{GFP}\rangle$ and $\langle \mathrm{ribo}\rangle$ are the mean GFP and ribosome concentrations and k_{tl} is the translation rate and the other variables are as previously defined. Next we develop expressions for the PSD of the transcriptional and translational extrinsic noise sources [these are analogous to Eq. (28)]:

$$S_{\mathrm{tc}}(f) \approx \frac{4\langle \mathrm{RNAP}\rangle}{\delta}\frac{1}{\left(1+\left(\frac{2\pi f}{\delta}\right)^2\right)}, \tag{36}$$

$$S_{\mathrm{tl}}(f) \approx \frac{4\langle \mathrm{ribo}\rangle}{\delta+k_{\mathrm{stalled}}}\frac{1}{\left(1+\left(\frac{2\pi f}{\delta+k_{\mathrm{stalled}}}\right)^2\right)}, \tag{37}$$

where $S_{\mathrm{tc}}(f)$ and $S_{\mathrm{tl}}(f)$ are the PSD of the transcriptional and translational extrinsic noise sources, $\langle \mathrm{RNAP}\rangle$ is the mean RNAP concentration, and k_{stalled} is the rate constant for dilution of ribosome stalled on transcripts. The following transfer functions describe the filtering of these noise sources through the gene circuit:

$$|H_{\mathrm{RNAP-GFP}}(f)|^2 = \left(\frac{k_{\mathrm{tc}}k_{\mathrm{tl}}\langle \mathrm{ribo}\rangle}{\gamma_m(\gamma_P+\delta)}\right)^2 \times \frac{1}{\left(1+\left(\frac{2\pi f}{\gamma_m}\right)^2\right)\left(1+\left(\frac{2\pi f}{\gamma_P+\delta}\right)^2\right)},$$
$$|H_{\mathrm{ribo-GFP}}(f)|^2 = \left(\frac{k_{\mathrm{tl}}\langle m\mathrm{RNA}\rangle}{(\gamma_P+\delta)}\right)^2 \frac{1}{\left(1+\left(\frac{2\pi f}{\gamma_P+\delta}\right)^2\right)}, \tag{38}$$

where k_{tc} is the transcription rate constant, and $|H_{\mathrm{RNAP\text{-}GFP}}(f)|^2$ and $|H_{\mathrm{ribo\text{-}GFP}}(f)|^2$ are the noise power transfer functions between the RNAP source and GFP output, and between the ribosome source and GFP output, respectively. As discussed earlier, the high frequency messenger RNA pole in Eq. (38) has little effect and is ignored in the remainder of this analysis. The PSDs of the GFP extrinsic noise components are obtained by multiplying the PSDs of the noise sources [Eqs. (36) and (37)] by the noise power transfer functions [Eq. (38)] to obtain:

$$S^{\mathrm{tc-ext}}_{\mathrm{GFP}}(f) \approx \frac{4\langle \mathrm{RNAP}\rangle}{\delta}\left(\frac{k_{\mathrm{tc}}k_{\mathrm{tl}}\langle \mathrm{ribo}\rangle}{\gamma_m(\gamma_P+\delta)}\right)^2 \times \frac{1}{\left(1+\left(\frac{2\pi f}{\delta}\right)^2\right)\left(1+\left(\frac{2\pi f}{\gamma_P+\delta}\right)^2\right)}, \tag{39}$$

$$S^{\mathrm{tl-ext}}_{\mathrm{GFP}}(f) \approx \frac{4\langle \mathrm{ribo}\rangle}{\delta+k_{\mathrm{stalled}}}\left(\frac{k_{\mathrm{tl}}\langle \mathrm{mRNA}\rangle}{(\gamma_P+\delta)}\right)^2 \times \frac{1}{\left(1+\left(\frac{2\pi f}{\delta+k_{\mathrm{stalled}}}\right)^2\right)\left(1+\left(\frac{2\pi f}{\gamma_P+\delta}\right)^2\right)}, \tag{40}$$

where $S^{\mathrm{tc\text{-}ext}}_{\mathrm{GFP}}(f)$ and $S^{\mathrm{tl\text{-}ext}}_{\mathrm{GFP}}(f)$ are the PSDs of the GFP noise due to transcriptional and translational level extrinsic sources. We now take the inverse Fourier transform of Eqs. (39), (40), and (35) to obtain the noise-source-specific GFP autocorrelation functions:

$$\Phi^{\mathrm{tc-ext}}_{\mathrm{GFP}}(\tau) = A^{\mathrm{tc-ext}}\left[\frac{\exp(-\delta\tau)}{\left[1-\left(\frac{\delta}{\gamma_p+\delta}\right)^2\right]} + \frac{(\gamma_p+\delta)}{\delta}\frac{\exp[-(\gamma_p+\delta)\tau]}{\left[1-\left(\frac{\gamma_p+\delta}{\delta}\right)^2\right]}\right],$$
$$\Phi^{\mathrm{tl-ext}}_{\mathrm{GFP}}(\tau) = A^{\mathrm{tl-ext}}\left[\frac{\exp[-(\delta+k_{\mathrm{stalled}})]}{\left[1-\left(\frac{\delta+k_{\mathrm{stalled}}}{\gamma_p+\delta}\right)^2\right]} + \frac{\gamma_p+\delta}{\delta+k_{\mathrm{stalled}}}\frac{\exp[-(\gamma_p+\delta)\tau]}{\left[1-\left(\frac{\gamma_p+\delta}{\delta+k_{\mathrm{stalled}}}\right)^2\right]}\right], \tag{41}$$

$$\Phi^{i}_{\mathrm{GFP}}(\tau) = A^{i}[\exp[-(\gamma_p + \delta)\tau]],$$

where the coefficients A are given by

$$A^{\mathrm{tc-ext}} = \frac{\langle \mathrm{GFP}\rangle^2}{\langle \mathrm{RNAP}\rangle},$$

$$A^{\mathrm{tl-ext}} = \frac{\langle \mathrm{GFP}\rangle^2}{\langle \mathrm{ribo}\rangle}, \tag{42}$$

$$A^{i} = \frac{\langle \mathrm{GFP}\rangle^2(\gamma_p + \delta)}{k_{\mathrm{tc}}\langle \mathrm{RNAP}\rangle}.$$

The total GFP autocorrelation function $\Phi_{\mathrm{GFP}}(\tau)$ is then given by the sum of the components:

$$\Phi_{\mathrm{GFP}}(\tau) = \Phi^{\mathrm{tc-ext}}_{\mathrm{GFP}}(\tau) + \Phi^{\mathrm{tl-ext}}_{\mathrm{GFP}}(\tau) + \Phi^{i}_{\mathrm{GFP}}(\tau). \tag{43}$$

The coefficients A reveal important insights concerning the relative importance of the three noise terms:

$$A^{\mathrm{tl-ext}} = A^{\mathrm{tc-ext}}\frac{\langle \mathrm{RNAP}\rangle}{\langle \mathrm{ribo}\rangle},$$

$$A^{i} = A^{\mathrm{tc-ext}}\frac{(\gamma_p + \delta)}{k_{\mathrm{tc}}}, \tag{44}$$

$$A^{\mathrm{tl-ext}} = A^{i}\frac{k_{\mathrm{tc}}}{(\gamma_p + \delta)}\frac{\langle \mathrm{RNAP}\rangle}{\langle \mathrm{ribo}\rangle}.$$

An increase in the $\langle \mathrm{RNAP}\rangle/\langle \mathrm{ribo}\rangle$ ratio increases the relative importance of translational level extrinsic noise relative to the other two sources. An increase in the ratio $(\gamma_p+\delta)/k_{\mathrm{tc}}$ increases the relative importance of intrinsic noise relative to the two extrinsic sources.

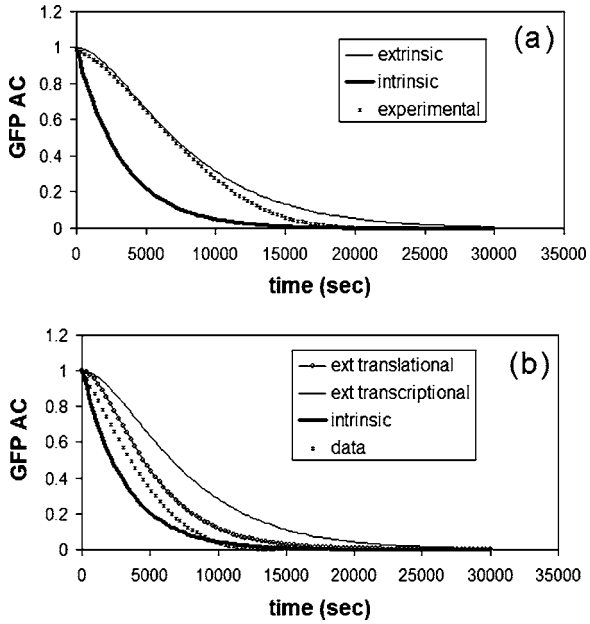

FIG. 9. Comparison of the experimental and source-specific normalized autocorrelation functions. The source-specific normalized autocorrelation functions were calculated from Eq. (45). (a) No ATc addition, doubling time 59 min and (b) 100 ng ml^{-1} ATc addition, doubling time 55 min.

Figure 9 shows normalized autocorrelation functions of GFP expression under conditions of similar doubling time both with [Fig. 9(a)] and without [Fig. 9(b)] ATc addition. Also shown in Fig. 9 are the normalized autocorrelation functions for transcriptional-extrinsic, translational-extrinsic and intrinsic noise sources, given by

$$\Phi^{\mathrm{ext-tc}}_{\mathrm{GFP\_}N}(\tau) = \frac{\Phi^{\mathrm{ext-tc}}_{\mathrm{GFP}}(\tau)}{\Phi^{\mathrm{ext-tc}}_{\mathrm{GFP}}(0)} = \frac{\left[1-\left(\frac{\gamma_p+\delta}{\delta}\right)^2\right]\exp(-\delta\tau) + \frac{(\gamma_p+\delta)}{\delta}\left[1-\left(\frac{\delta}{\gamma_p+\delta}\right)^2\right]\exp[-(\gamma_p+\delta)\tau]}{\left[1-\left(\frac{\gamma_p+\delta}{\delta}\right)^2\right] + \frac{(\gamma_p+\delta)}{\delta}\left[1-\left(\frac{\delta}{\gamma_p+\delta}\right)^2\right]},$$

$$\Phi^{\mathrm{ext-tl}}_{\mathrm{GFP\_}N}(\tau) = \frac{\Phi^{\mathrm{ext-tl}}_{\mathrm{GFP}}(\tau)}{\Phi^{\mathrm{ext-tl}}_{\mathrm{GFP}}(0)} = \frac{\left[1-\left(\frac{\gamma_p+\delta}{\delta+k_{\mathrm{stall}}}\right)^2\right]\exp(-(\delta+k_{\mathrm{stall}})\tau) + \frac{(\gamma_p+\delta)}{\delta+k_{\mathrm{stall}}}\left[1-\left(\frac{\delta+k_{\mathrm{stall}}}{\gamma_p+\delta}\right)^2\right]\exp[-(\gamma_p+\delta)\tau]}{\left[1-\left(\frac{\gamma_p+\delta}{\delta+k_{\mathrm{stall}}}\right)^2\right] + \frac{(\gamma_p+\delta)}{\delta+k_{\mathrm{stall}}}\left[1-\left(\frac{\delta+k_{stall}}{\gamma_p+\delta}\right)^2\right]}, \tag{45}$$

$$\Phi^{i}_{\mathrm{GFP\_}N}(\tau) = \frac{\Phi^{\mathrm{int}}_{\mathrm{GFP}}(\tau)}{\Phi^{\mathrm{int}}_{\mathrm{GFP}}(0)} = \exp[-(\gamma_p+\delta)\tau].$$

The experimental curves can be thought of as a mixture of the normalized noise-source-specific ACFs given in Eq. (45). It is also noteworthy that the noise-source-specific curves are determined entirely by the predominant pole frequencies in the system (δ, $\gamma_p+\delta$, and $\delta+k_{\mathrm{stalled}}$). In these plots, the protein half-life is taken to be 110 min and the cell doubling times are as indicated in Fig. 9. We also assume that k_{stalled} in the presence of ATc is approximately equal to the cell doubling rate δ corresponding to the experimental observation that at constant temperature the cell growth rate decreases by

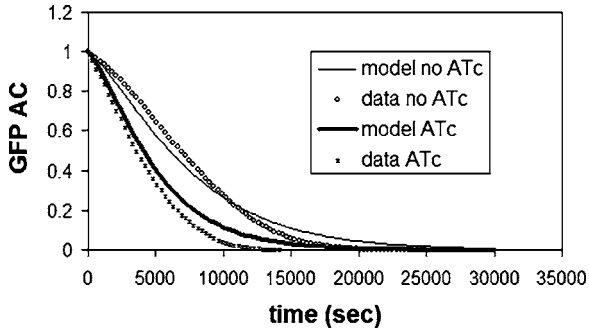

FIG. 10. The effect of ATc addition on the normalized autocorrelation function of GFP expression noise. The solid lines represent model predictions based on Eq. (43), whereas the symbols represent experimental data [no ATc addition, doubling time 59 min; ATc addition (100 ng ml^{-1}), doubling time 55 min].

about a factor of 2 upon addition of ATc. When no ATc is present, $k_{\text{stalled}}=0$ and the normalized ACFs for the two extrinsic sources are identical. In this case, the experimental data closely follows the extrinsic noise autocorrelation function. Upon addition of ATc, the stalling of ribosomes on mRNA shifts the autocorrelation function of translational extrinsic noise to the left (i.e., a shift of the PSD to higher frequencies in the frequency domain), whereas the autocorrelation functions of the other two noise sources are largely unaffected by the slight change in δ. The experimental data now fall between the theoretical curves for the extrinsic translational noise and the intrinsic noise. It should be noted that only the early portions ($\tau \leqslant \tau \leqslant \tau_{1/2}$) of the experimental autocorrelation functions are likely to be accurate, due to the limited experimental duration (7 h without ATc and 4 h with ATc). Another factor limiting the accuracy of the experimental curve is the use of the biased autocorrelation function in processing the experimental data, which forces the autocorrelation function to approach zero at a τ equal to the experimental duration.

In order to compare the autocorrelation function for the total noise to the experimental autocorrelation functions we must first assign values to the parameters that determine the weighting factors. Inspection of Eq. (44) reveals that the weighting coefficients will depend on only two additional independent parameters: $\langle \text{RNAP} \rangle / \langle \text{ribo} \rangle$ and k_{tc}. Inspection of Fig. 9(b) reveals that extrinsic translational noise should be weighted more heavily than extrinsic transcription noise and that intrinsic noise should play at least a moderate role. Based on these observations we set $\langle \text{RNAP} \rangle / \langle \text{ribo} \rangle = 10$ and $k_{\text{tc}}=2\times10^{-4}$ s^{-1}, yielding reasonable fits to the experimental data observed in Fig. 10. The model reveals two predominant effects of ATc addition. First the ACF for the translational extrinsic noise is shifted to the left as a result of the increase in pole frequency due to k_{stalled}. Second, the absolute magnitude of the contribution of this noise source to the total ACF decreases with increasing k_{stalled}, as seen in Eq. (41).

To model the addition of ATc in Fig. 10, only the values of k_{stalled} and δ were modified as described previously. However, the effects of changes in other parameters should be considered. In the model development we mentioned that the effect of increasing mRNA stability could be incorporated by increasing γ_m upon addition of ATc. Further, we suggested that stalled ribosomes could reduce the transcription initiation rate k_{tl} by blocking the ribosome binding site. However, neither of the parameters appears either directly or indirectly in the normalized GFP ACFs. Ribosome stalling is expected to decrease the activity of ribosomes and could act to increase the ratio $\langle \text{RNAP} \rangle / \langle \text{ribo} \rangle$. This would tend to move the model ACF to the right (i.e., a shift in the PSD to lower frequencies in the frequency domain), away from the experimental data. However, as RNAP synthesis is dependent upon ribosome activity it can be expected that the decrease in ribosome activity will be at least partially offset by a decrease in RNAP activity. The ATc experiment was conducted at a higher temperature (30 °C, compared to 26 °C without ATc) to achieve a near constant growth rate. A temperature-related increase in the transcription rate constant k_{tc} again moves the model ACF to lower frequencies away from the experimental data, but the effect is relatively modest even with a twofold increase in the rate constant. In our earlier work, we assumed that the protein decay rate constant γ_p was independent of temperature. An increase in this rate constant with temperature would tend to shift the analytical curve to higher frequencies and closer to the experimental data. Cumulatively, the effect of these considerations was modest and within the experimental error of the data.

This frequency domain analysis of extrinsic and intrinsic noise sources and their propagation through gene circuits suggests that translational extrinsic noise is the most dominant noise source in the system investigated here, with intrinsic noise playing an important secondary role. Much more theoretical and experimental work is needed to gain a basic characterization of extrinsic noise sources and their effects. The frequency domain analysis presented here provides a convenient framework for planning and interpreting experimental efforts with this goal.

VII. CONCLUSIONS

Phenotypic variability not originating from genetic or environmental causes has been long observed in biology, but experimental capabilities to investigate these stochastic mechanisms at the molecular level have only been developed in recent years. Most studies of genetic noise to date have focused on its magnitude. In this article, we have summarized our recent work that demonstrates that the frequency content of gene noise contains additional information that can provide insight into the structure and function of gene networks. We also presented an expanded model to explain the experimentally observed ATc-mediated frequency shift in gene noise that explicitly considers extrinsic noise at the transcriptional and translational levels. We envision future work in this area will make significant contributions to a generalized understanding of gene networks. Progress is expected in better understanding of the sources and propagation of intrinsic noise in gene circuits and the characteristic noise signatures of various regulatory motifs. We also expect continued progress in understanding how specific cellular systems exploit noise dynamics to achieve desired phenotypes. For example, a recent study has identified a core network of genes that controls the spontaneous and stochastic

entry of *Bacillus subtlis* into a competent state and its subsequent exit from that state.[45] An interesting unanswered question is the relationship between the frequency of the competence initiation and exit events and the values of kinetic parameters in the gene network.

ACKNOWLEDGMENTS

This work was supported by the DARPA Bio-Computation Program, the NSF (Award EIA-0130843) and the National Academies Keck Futures Initiative. D.W.A. acknowledges support from an ORNL Center for Nanophase Materials Sciences Research Scholar Fellowship. R.D.D. acknowledges support from the DOE Science Undergraduate Laboratory Internship program.

[1]M. Delbruck, J. Chem. Phys. **8**, 120 (1940).
[2]M. Delbruck, J. Bacteriol. **50**, 131 (1945).
[3]A. Novick and M. Weiner, Proc. Natl. Acad. Sci. U.S.A. **43**, 553 (1957).
[4]M. Ptashne, *A Genetic Switch: Gene Control and Phage Lambda* (Cell Press, Cambridge, MA, 1986).
[5]A. Arkin, J. Ross, and H. H. McAdams, Genetics **149**, 1633 (1998).
[6]J. L. Spudich and D. E. KoshlandJr., Nature (London) **262**, 467 (1976).
[7]A. Colman-Lerner, A. Gordon, E. Serra, T. Chin, O. Resnekov, D. Endy, C. G. Pesce, and R. Brent, Nature (London) **437**, 699 (2005).
[8]P. Simpson, Curr. Opin. Genet. Dev. **7**, 537 (1997).
[9]M. Thattai and A. van Oudenaarden, Genetics **167**, 523 (2004); E. Kussell and S. Leibler, Science **309**, 2075 (2005).
[10]C. V. Rao, D. M. Wolf, and A. P. Arkin, Nature (London) **420**, 231 (2002).
[11]M. Kaern, T. C. Elston, W. J. Blake, and J. J. Collins, Nat. Rev. Genet. **6** (6), 451 (2005); J. M. Raser and E. K. O'Shea, Science **309**, 2010 (2005).
[12]M. B. Elowitz, A. J. Levine, E. D. Siggia, and P. S. Swain, Science **297**, 1183 (2002).
[13]P. S. Swain, M. B. Elowitz, and E. D. Siggia, Proc. Natl. Acad. Sci. U.S.A. **99**, 12795 (2002).
[14]J. M. Pedraza and A. van Oudenaarden, Science **307**, 1965 (2005).
[15]M. A. Gibson and J. Bruck, J. Phys. Chem. A **104**, 1876 (2000).
[16]D. T. Gillespie, J. Comput. Phys. **22**, 403 (1976).
[17]D. T. Gillespie, J. Phys. Chem. **81**, 2340 (1977).
[18]D. T. Gillespie, Physica A **188**, 404 (1992).
[19]D. T. Gillespie, J. Chem. Phys. **113**, 297 (2000).
[20]D. T. Gillespie, W. O. Alltop, and J. M. Martin, Chaos **11**, 548 (2001); J. Hasty, D. McMillen, F. Isaacs, and J. J. Collins, Nat. Rev. Genet. **2**, 268 (2001); H. H. McAdams and A. Arkin, Annu. Rev. Biophys. Biomol. Struct. **27**, 199 (1998); C. V. Rao and A. P. Arkin, J. Chem. Phys. **118**, 4999 (2003).
[21]T. B. Kepler and T. C. Elston, Biophys. J. **81**, 3116 (2001).
[22]E. M. Ozbudak, M. Thattai, I. Kurtser, A. D. Grossman, and A. van Oudenaarden, Nat. Genet. **31**, 69 (2002).
[23]M. Thattai and A. van Oudenaarden, Proc. Natl. Acad. Sci. U.S.A. **98**, 8614 (2001).
[24]M. L. Simpson, C. D. Cox, and G. S. Sayler, Proc. Natl. Acad. Sci. U.S.A. **100**, 4551 (2003).
[25]M. L. Simpson, C. D. Cox, and G. S. Sayler, J. Theor. Biol. **229**, 383 (2004).
[26]C. D. Cox, G. D. Peterson, M. S. Allen, J. M. Lancaster, J. M. McCollum, D. Austin, L. Yan, G. S. Sayler, and M. L. Simpson, Omics, a Journal of Integrative Biology **7**, 317 (2003).
[27]J. Hasty, J. Pradines, M. Dolnik, and J. J. Collins, Proc. Natl. Acad. Sci. U.S.A. **97**, 2075 (2000); D. T. Gillespie, J. Phys. Chem. A **106**, 5063 (2002).
[28]W. J. Blake, M. Kaern, C. R. Cantor, and J. J. Collins, Nature (London) **422**, 633 (2003).
[29]J. M. Raser and E. K. O'Shea, Science **304**, 1811 (2004).
[30]A. Becskei and I. W. Mattaj, Curr. Opin. Cell Biol. **17**, 27 (2005).
[31]N. Rosenfeld, J. W. Young, U. Alon, P. S. Swain, and M. B. Elowitz, Science **307**, 1962 (2005).
[32]D. W. Austin, M. S. Allen, J. M. McCollum, R. D. Dar, J. W. Wilgus, G. S. Sayler, N. F. Samatova, C. D. Cox, and M. L. Simpson, Nature (London) **439** (7076), 608 (2006).
[33]G. Stephanopoulos, A. Aristidou, and J. Nielsen, *Metabolic Engineering: Principals and Methodologies* (Academic, New York, 1998).
[34]T. S. Gardner, C. R. Cantor, and J. J. Collins, Nature (London) **403**, 339 (2000).
[35]M. B. Elowitz and S. Leibler, Nature (London) **403**, 335 (2000).
[36]D. Volfson, J. Marciniak, W. J. Blake, N. Ostroff, L. S. Tsimring, and J. Hasty, Nature (London) **439**, 861(2006).
[37]Y. Cao, H. Li, and L. R. Petzold, J. Chem. Phys. **121**, 4059 (2004).
[38]J. M. McCollum, G. D. Peterson, C. D. Cox, M. L. Simpson, and N. F. Samatova, Comput. Biol. Chem. **30**, 39 (2006).
[39]J. S. Bendat and A. B. Piersol, *Random Data: Analysis and Measurement Procedures* (Wiley, New York, 2000).
[40]J. B. Andersen, C. Sternberg, L. K. Poulsen, S. P. Bjørn, M. Givskov, and S. Molin, Appl. Environ. Microbiol. **64**, 2240 (1998).
[41]R. Lutz and H. Bujard, Nucleic Acids Res. **25**, 1203 (1997).
[42]I. Chopra and M. Roberts, Microbiol. Mol. Biol. Rev. **65**, 232 (2001).
[43]C. Petersen, in *Control of Messenger RNA Stability*, edited by J. G. Belasco and G. Brawerman (Academic, San Diego, 1993), pp. 117–145.
[44]P. J. Lopez, I. Marchand, O. Yarchuk, and M. Dreyfus, Proc. Natl. Acad. Sci. U.S.A. **95**, 6067 (1998).
[45]G. M. Süel, J. Garcia-Ojalvo, L. M. Liberman, and M. B. Elowitz, Nature (London) **440**, 545 (2006).